nature neuroscience

ARTICLES

https://doi.org/10.1038/s41593-018-0175-4

A 3D human triculture system modeling neurodegeneration and neuroinflammation in Alzheimer's disease

Joseph Park[1,2,3,4,5], Isaac Wetzel[1,2,3,4], Ian Marriott[2,3], Didier Dréau[2,3], Carla D'Avanzo[5], Doo Yeon Kim[5*], Rudolph E. Tanzi[5*] and Hansang Cho[1,2,3,4*]

Alzheimer's disease (AD) is characterized by beta-amyloid accumulation, phosphorylated tau formation, hyperactivation of glial cells, and neuronal loss. The mechanisms of AD pathogenesis, however, remain poorly understood, partially due to the lack of relevant models that can comprehensively recapitulate multistage intercellular interactions in human AD brains. Here we present a new three-dimensional (3D) human AD triculture model using neurons, astrocytes, and microglia in a 3D microfluidic platform. Our model provided key representative AD features: beta-amyloid aggregation, phosphorylated tau accumulation, and neuroinflammatory activity. In particular, the model mirrored microglial recruitment, neurotoxic activities such as axonal cleavage, and NO release damaging AD neurons and astrocytes. Our model will serve to facilitate the development of more precise human brain models for basic mechanistic studies in neural–glial interactions and drug discovery.

Alzheimer's disease (AD) is the leading cause of age-related neurodegeneration, affecting over 5.2 million people in the United States alone[1]. Our knowledge regarding mechanisms underlying the AD pathogenesis has greatly improved in the last decades, but still there is no cure[1]. Moreover, many unanswered questions have remained regarding the pathogenic cascade of AD, including reactive gliosis and the related neuronal damages[2–4]. Recent advances in cell reprograming allow the study of human neurons derived from AD patient fibroblasts[5–14]. These fibroblast-derived neurons share the genetic material of AD patients and provide an excellent tool for recapitulating the pathogenic cascades of AD in human brain environment[10–14]. Indeed, familial and sporadic AD neurons derived from human induced pluripotent stem cells (iPSCs) exhibit relatively high levels of beta-amyloid 40 (Aβ40) and phosphorylated tau (p-tau) compared to controls[14]. Furthermore, we previously reported a 3D culture model of AD using human neural progenitor cells overexpressing APP and PSEN1 with human familial AD (FAD) mutations[15,16]. When seeded in a novel 3D culture system, these cells demonstrated robust extracellular aggregates of Aβ (Aβ-plaque-like) and Aβ-induced pathological tau aggregation (NFT-like)[15–18]. While this 3D model successfully recapitulated key pathological hallmarks of AD, it did not contain a neuroinflammatory component, which is the essential pathological event observed in human AD patients and AD mouse models.

The next challenge is the generation of a human AD culture model that includes neuroinflammation, a key component of neurodegenerative disorders commonly induced through activation of microglia and astrocytes. The sustained activation of microglia results in a chronic neuroinflammatory response and increased production of proinflammatory cytokines, such as TNF-α and IL-1β[19]. Of relevance, recent genome-wide association studies have uncovered several risk-associated genes in the development of sporadic AD. Most of these risk genes are either expressed by microglia or associated with their reactivity, including CD33[20], BIN1[21], CR1[22], TREM2[23], and CLU[24]. As such, there is a pressing need for the development of organotypic models to detail cellular mechanisms and recapitulate the complex neural–glial interactions in AD.

Here we present an engineered model of neuron (Neu)+ astrocyte (AC) + microglia (MG) interaction in AD environment (Neu+AC+MG AD) that enables the study of human microglia recruitment, neuroinflammatory response, and damage to neurons and/or astrocytes (neurons/astrocytes). To achieve this, we built a human triculture system in which neurons and astrocytes differentiated first, and then added adult microglia cells at different stages of AD. This new 3D human AD triculture system demonstrated Aβ aggregation and p-tau formation along with increased chemokines and cytokines, including CCL2, IL8, TNF-α , and IFN-γ. Notably, 3D Neu+AC AD culture induced microglia recruitment and led to marked neuron/astrocyte loss. Together, these results suggest that our new 3D human AD triculture system provides a valid model for investigating complex neuroinflammatory molecular mechanisms underlying AD pathology and may contribute to finding new therapeutic targets.

Results

Generation of human AD triculture system (Neu+AC+MG AD) using a microfluidic platform. The AD brain platform used here consists of a microfluidic device containing two chambers mimicking the in vivo AD environment to observe interactions between neurons/astrocytes and microglia. The central chamber was loaded with the 3D AD neuron/astrocyte differentiated cells, while the angular chamber was loaded with adult microglia (Fig. 1a–c). Human neural

[1]Department of Mechanical Engineering and Engineering Science, University of North Carolina at Charlotte, Charlotte, NC, USA. [2]Center for Biomedical Engineering and Science, University of North Carolina at Charlotte, Charlotte, NC, USA. [3]Department of Biological Sciences, University of North Carolina at Charlotte, Charlotte, NC, USA. [4]The Nanoscale Science Program, University of North Carolina at Charlotte, Charlotte, NC, USA. [5]Genetics and Aging Research Unit, MassGeneral Institute for Neurodegenerative Disease, Massachusetts General Hospital, Harvard Medical School, Charlestown, MA, USA. *e-mail: dkim@helix.mgh.harvard.edu; tanzi@helix.mgh.harvard.edu; h.cho@uncc.edu

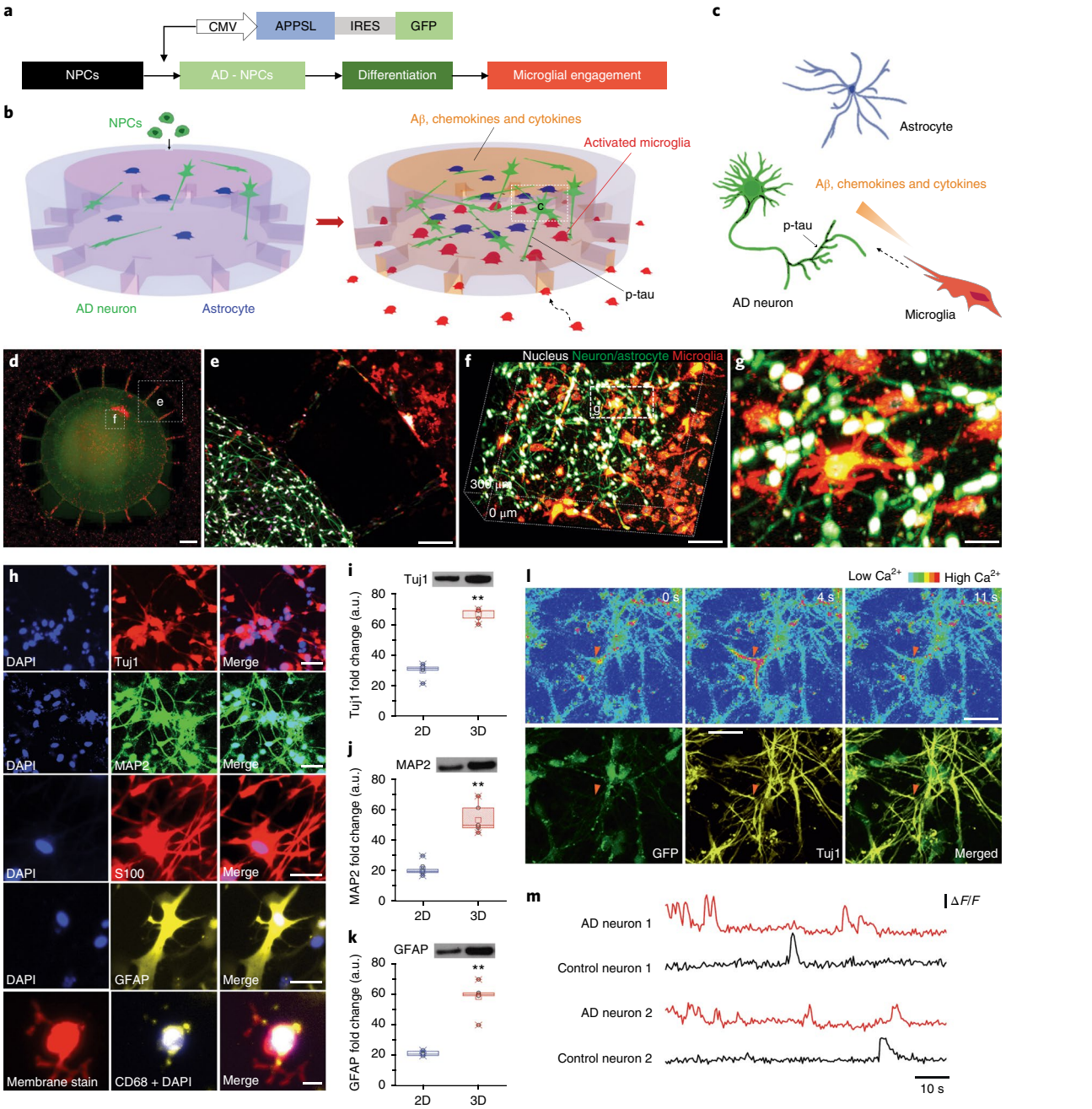

Fig. 1 | Construction of a 3D organotypic human AD culture model (3D Neu + AC + MG AD): a triculturing system of AD neurons, astrocytes differentiated from hNPCs, and human adult microglia in a 3D microfluidic platform. **a**, Schematic of differentiation of NPCs to AD neuron/astrocyte and microglial engagement. CMV, human cytomegalovirus. **b**,**c**, Schematics showing multicellular 3D layouts in (**b**) a microfluidic human AD culture model and (**c**) human AD brain tissue. **d**, Fluorescent microphotographs show the layout of human AD neurons/astrocytes (green) in a central chamber and microglia (red) in angular chambers. Scale bar, 250 µm. **e**, Microglia are recruited across microchannels between the central chamber and the angular chambers by soluble factors from the AD culture cells. Scale bar, 250 µm. **f**,**g**, Representative confocal microphotographs in the central chamber highlight the physiological 3D cellular engagement of neurons (green), astrocyte (green), and microglia (red) with nuclear staining (white). Scale bars, 100 µm in **f**; 40 µm in **g**. **h**, Immunofluorescent microphotographs validate the differentiated neurons (blue, nucleus) with class III β-tubulin Tuj1 (red) and MAP2 (green), astrocytes (blue, nucleus) with S100 (red) and GFAP (yellow), and the recruited microglia (blue, nucleus; red, prestained membrane) with CD68 (yellow). Scale bars, 40 µm for Tuj1 and MAP2; 20 µm for S100, GFAP, and CD68. **i**–**k**, Western blot assay demonstrates the increased expression of neuronal markers (Tuj1: $t = 9.105$, df = 5.24, $R^2 = 0.9405$, $F = 41.68$, $P = 0.0009$, $n = 20$ devices from 3-week 1:1 thick-culture condition; MAP2: $t = 25.64$, df = 7.526, $R^2 = 0.9887$, $F = 1.67$, $P = 0.0027$, $n = 20$ devices from 3-week 1:1 thick-culture condition) and astrocyte markers (GFAP: $t = 12.58$, df = 7.828, $R^2 = 0.9529$, $F = 1.349$, $P = 0.0019$, $n = 20$ devices from 3-week 1:1 thick-culture condition) of the 3D culture system compared to a 2D culture after 3 weeks of differentiation. Data are normalized to undifferentiated hNPCs. All experiments were repeated ≥3 times statistics represent unpaired, two-sided Student's *t* tests; $^{**}P < 0.01$. **l**, Time-lapse microphotographs show calcium signaling with Cal590 fluorescent dyes from firing neurons (top; orange triangle) and are compared with immunostained neuronal marker of Tuj1 in yellow and membrane in green (bottom). Scale bar, 50 µm. **m**, Normalized values ($\Delta F/F$) from neurons representative for control and for the AD model after 3 weeks of differentiation indicate functionally connected neuronal activities. All experiments were repeated ≥3 times; all parameters are presented as mean ± s.e.m.

progenitor cells (ReNcell VM cells, an immortalized human neural progenitor cell line; hereafter referred to as hNPCs) that produce high levels of Aβ were developed through overexpression of a variant of the human Aβ precursor protein (APP) containing FAD mutations with both K670N/M671L (Swedish) and V717I (London) FAD mutations (APPSL) under the human cytomegalovirus immediate-early enhancer and promoter, as previously published (Supplementary Fig. 1)[15]. These transduced cells with control-GFP (Neu+AC) or APPSL-GFP (Neu+AC AD) lentiviral particles were enriched on the basis of GFP signals through fluorescence-activated cell sorting. Representative fluorescence microphotographs of differentiated ReN cells showed stable expression for more than 3 weeks (control-GFP: Neu + AC and APPSL-GFP: Neu + AC AD; Supplementary Fig. 1). The central and angular chambers were linked by migration channels (10 × 50 × 500 μm, height × width × length) forming gradients of soluble factors. These long, thin migration channels prevented inadvertent entrance of inactivated microglia through mechanical constraints. Using this platform, we observed the migration of microglial cells, at single-cell resolution, in real time for extended periods (Fig. 1d). hNPCs, differentiated into neuron and astrocyte, were successfully tricultured with adult microglia (Fig. 1d–g). These observations demonstrated that our 3D microfluidic device enabled the formation of physiologically relevant human brain tissue-mimetic 3D structures (Supplementary Fig. 2).

To demonstrate hNPCs differentiation in 3D cultures (Supplementary Videos 1 and 2), fixed cells were analyzed by immunofluorescence for the presence of neuronal/astrocyte markers. As previously reported, hNPCs robustly expressed class III beta-tubulin (Tuj1), microtubule-associated protein 2 (MAP2), glial fibrillary acidic protein (GFAP), and calcium-binding proteins (S100, S100A6, and S100β) in week 3 (Fig. 1h and Supplementary Figs. 3 and 4)[15]. Activated microglia, as demonstrated by CD68 expression, were also observed in triculture conditions in the 3D Neu+AC+MG AD culture model (Fig. 1h). Neuronal (Tuj1, MAP2) and glial (GFAP) markers in undifferentiated and 3-week differentiated AD hNPCs were quantified by western blot analysis (Fig. 1i–k). Western blot analysis for neuronal markers Tuj1 and MAP2, and for the astrocytic marker GFAP, demonstrated that neuronal and astrocyte differentiation of NPCs was significantly promoted, by 2.1-fold, 2.9-fold, and 2.3-fold, respectively, in 3D culture in microfluidic devices compared to 2D cultures. These differences may reflect the ability of 3D environments to promote differentiation and/or maturation of neural progenitor cells providing a high surface area for growth[25,26].

We next characterized action potential-evoked calcium dynamics in individual neurons (Fig. 1l) filled with Cal-590[27]. The recorded individual neurons were immunoassayed with the neuronal marker Tuj1 to confirm that the calcium dynamics was from neurons. High-magnification microphotographs of the soma of stained neurons displayed the characteristic ring shape arising from a lower fluorescence level in the nucleus compared with the surrounding cytoplasm (Supplementary Fig. 5). We analyzed the spontaneous activity of these neurons by combining calcium activation, neuronal markers, and fast time-lapse imaging (50 frames per unit time) and found that calcium transients evoked by individual action potentials were discernible with a good signal-to-noise ratio (Fig. 1m and Supplementary Video 3)[27]. Notably, 3D Neu+AC AD showed a substantial increase of neuronal activity levels that could be observed when compared with week-matched control (3D Neu+AC) in the 3-week-old cells. Furthermore, the fraction of neurons that were hyperactive (>6 transients per 60 s) was markedly larger in 9-week-old 3D Neu+AC AD than in 3-week-old 3D Neu+AC AD, while the fraction of silent neurons (0 transients per 30 s) was not different between 3D Neu+AC AD at week 3 and week 9 (Supplementary Fig. 6 and Supplementary Videos 4 and 5). Taken together, these data clearly demonstrate the generation of functional neuron/astrocyte cell models in our 3D microfluidic culture system.

Increased soluble Aβ, inflammatory cytokines/chemokines, and p-tau in the 3D Neu+AC AD model. The levels of soluble 40-amino acid and 42-amino acid Aβ isoforms (Aβ40 and Aβ42) were determined in conditioned media collected after 3, 6, and 9 weeks of differentiation in either 2D or 3D cultures of control neuron/astrocyte (Neu + AC) or AD neuron/astrocyte (Neu + AC AD) cells. Aβ40 (changed by 10.2-fold and 1.7-fold) and Aβ42 (changed by 8.2-fold and 1.1-fold) levels were compared to the control 3D Neu + AC and 2D Neu + AC AD (Fig. 2a,b) at week 3. Furthermore, at week 9, 3D Neu + AC AD was associated with significantly higher accumulations of Aβ40 (78-fold and 2.8-fold compared to levels observed in 3D Neu + AC and 2D Neu + AC AD, respectively). Notably, the soluble Aβ42 week 9/week 0 ratio in 3D Neu + AC AD was substantially decreased (≈ 20%), indicating that the 3D culture conditions may increase the aggregation of Aβ42 (Fig. 2a,b and Supplementary Figs. 7 and 8). This observation was further validated through western blot analysis of the various forms of aggregated Aβ in whole lysates (Fig. 2c,d), with increased aggregated forms of Aβ found in 3D Neu + AC AD[28]. These observations are consistent with an accelerated Aβ accumulation due to limited diffusion in 3D culture conditions and diffusion of AD neuron-derived Aβ into the media in 2D cultures as previously reported[15,16].

To determine whether our 3D Neu + AC AD secretes CCL2 (MCP-1), a chemokine upregulated in AD brains, we compared the level of CCL2 in various stages of the AD culture models[29]. We found that 3D Neu + AC AD (1,800 pg/mL) showed 2.9-fold and 1.3-fold more CCL2 secretion in conditioned media compared to 3D Neu + AC (620 pg/mL) and 2D Neu + AC AD (1,384 pg/mL), respectively (Fig. 2e). To further explore pathology development in 3D cultured AD neurons/astrocytes, chemokine and cytokine secretion by 3D Neu + AC, 2D Neu + AC AD, and 3D Neu + AC AD cells was determined. First, we evaluated TNF-α levels in the culture medium and found TNF-α levels increased by 2.8-fold and 8.2-fold in week 6 (61 pg/mL) and week 9 (180 pg/mL), respectively, in 3D Neu + AC AD (Fig. 2f), while moderate increases were observed in 2D Neu + AC AD. Unexpectedly, IFN-γ was exclusively secreted by 3D Neu + AC AD cells (9.2 pg/mL) but not detected in the other conditions tested (Fig. 2g).

Regarding tau alterations[30], Enzyme-linked immunosorbent assay (ELISA) of soluble p-tau (pSer231 tau; phosphorylated at Serine 231) in 3D Neu + AC AD cells showed that pSer231 tau levels increased by 2.2-fold and 5.1-fold at weeks 6 (271 pg/mL) and 9 (630 pg/mL), respectively, compared to 3D Neu + AC (Fig. 2h). The presence of p-tau phosphorylation at Ser396 and Ser404 and at Ser202 and Thr206 was also confirmed by immunofluorescent staining using the p-tau antibodies PHF-1 and AT8, respectively, in both neuritic and soma bodies of 3D Neu+AC AD cells (Fig. 2i and Supplementary Fig. 9).

3D Neu+AC AD model induced microglial migration, phenotype changes, and secretion of pro-inflammatory factors. To test the hypothesis that neurons/astrocytes in AD environments induce activation and/or recruitment of microglial cells, we plated microglial cells in the angular chamber at day 0 of week 3, week 6, and week 9. To characterize the migration and phenotype changes of microglia, individual microglial cells were monitored for 7 d using time-lapse imaging microscopy (Fig. 3a). In the first 24 h, microglia in the angular chamber showed widely branched filopodia in all directions, a morphology typically associated with 'resting' microglia. Furthermore, most of the cells remained stationary during that period. Morphological changes and microglial migration toward the central chamber seeded with 3D Neu + AC AD was observed 48 h after cell seeding (Fig. 3b). As determined by image analysis, microglial cells became elongated, with substantially increased cell length and microglial cell body area (Fig. 3b,c). Furthermore, exposure of microglia to 3D Neu + AC AD induced upregulation

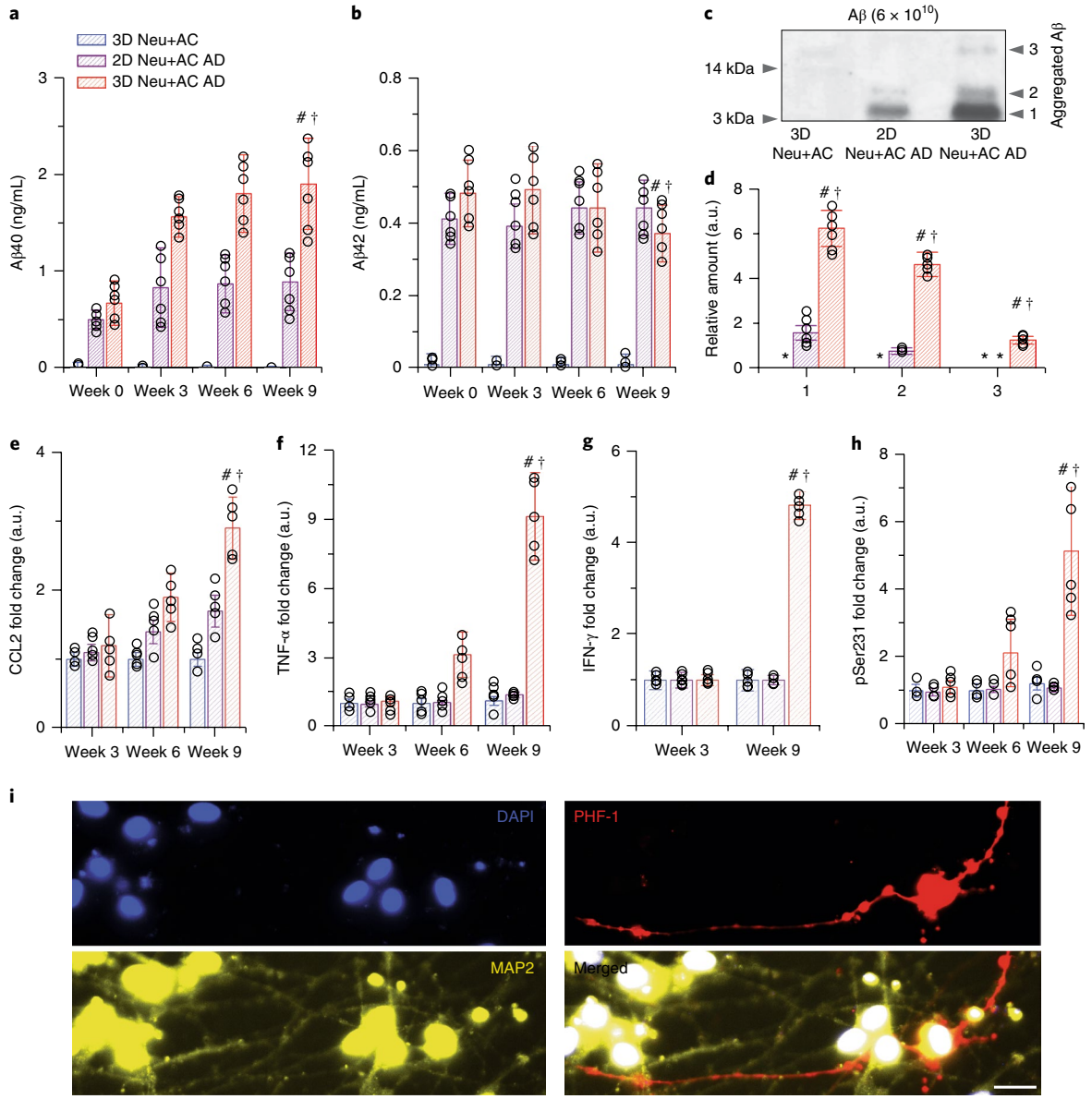

Fig. 2 | Recapitulation of pathological AD signatures: Aβ, p-tau, and IFN-γ in the 3D Neu + AC AD model. a,**b**, Soluble (**a**) Aβ40 and (**b**) Aβ42 were measured after 0, 3, 6, and 9 weeks of differentiation in a 3D control model (3D Neu + AC), 2D AD model (2D Neu + AC AD), and 3D AD model (3D Neu + AC AD; $n = 6$ devices from 3-week 1:1 thick-culture condition). **c**, Western blot analysis confirms the presence of sodium dodecyl sulfate (SDS)-resistant Aβ multimeric forms in 3D Neu + AC AD. All experiments were repeated ≥3 times. **d**, Quantification of elevated levels of multiple forms shown in Fig. 3c ($F_{2,9} = 530.6$, $SS = 6.438$). **e**,**f**, Noticeable increases of (**e**) CCL2 ($R^2 = 0.9804$, $F_{2,12} = 300.6$) and (**f**) TNF-α were observed in the 3D Neu + AC AD model ($R^2 = 0.9953$, $F_{2,12} = 1{,}271$). **g**–**i**, Accumulations of (**g**) IFN-γ ($R^2 = 0.7584$, $F_{2,12} = 18.84$), (**h**) soluble p-tau (pSer231 tau, $R^2 = 0.9235$, $F_{2,12} = 72.39$), and (**i**) p-tau (PHF-1; red) in neuronal cell bodies and neurites (green) were observed only after 9 weeks in the 3D Neu + AC AD model. Scale bar, 25 μm. All experiments were repeated ≥ 3 times; statistics reflect one-way ANOVA with Tukey–Kramer tests, $n = 5$ devices each; significance is denoted by week-9 3D Neu + AC vs. week-9 3D Neu + AC AD, $^{\#}P < 0.001$; week-9 2D Neu + AC + MG AD vs. week-9 3D Neu + AC + MG AD, $^{\dagger}P < 0.001$; * indicates not detected.

of microglial activation markers such as CD11b (Fig. 3d). The migration rate of microglial cells in the 3D Neu + AC + MG AD environment was substantially higher compared with those in the other conditions tested, 3D Neu + AC + MG or 2D Neu + AC + MG AD. The microglial recruitment index (Supplementary Fig. 10) was 8.1 ± 0.78% in 3D Neu + AC + MG AD cells compared with 4.2 ± 2.3% in 2D Neu + AC + MG AD cells and 0.9 ± 1.2% in 3D Neu + AC + MG cells (Fig. 3e). Notably, neutralization of CCL2 chemokine signaling using an antibody against CCL2 reduced the ability of microglia to migrate in response to Neu + AC AD co-culture conditions (Supplementary Fig. 11). Other factors, such as ATP[31] (Supplementary Fig. 12), may also contribute to microglial recruitment in our system. Notably, in the 3D Neu + AC + MG AD model, the aged cultures (week 9) led to the recruitment of more microglia cells as compared to early-stage cultures. 3D Neu + AC + MG AD and 2D Neu + AC + MG AD culture platforms had comparable effects on maximal microglial migration speed (5.0 ± 0.91 vs. 4. 3 ± 0.81; data not shown). The observed speed of migration (μm/h) was similar to that previously observed in AD environments with soluble and bound Aβ conditions[15].

Next, we set out to identify the cytokines and chemokines that regulate the microglial migration and activation in our 3D AD

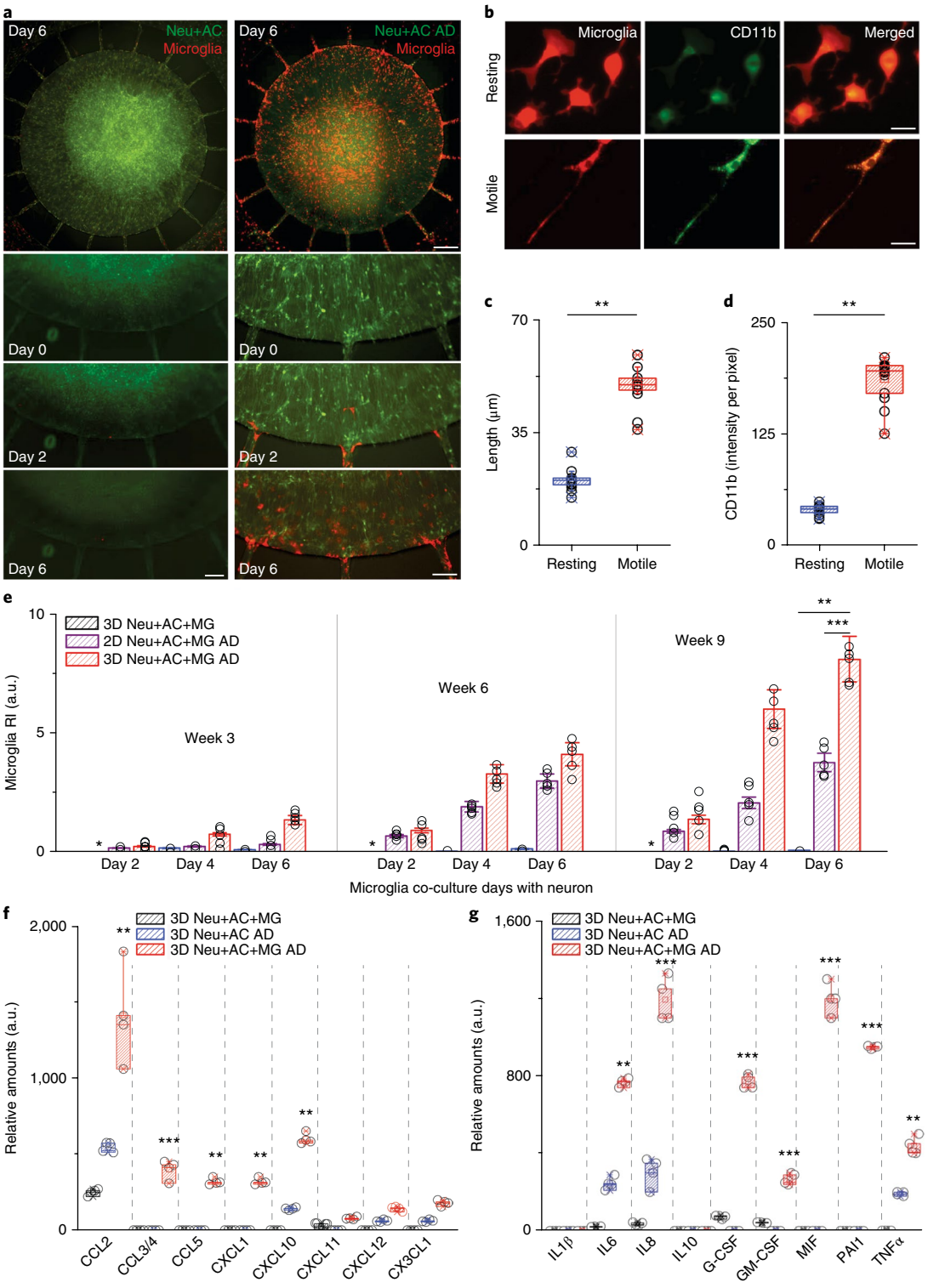

Fig. 3 | Activation of microglial inflammation: morphogenesis, marker expression, recruitment, and inflammatory mediator release. a, Time-lapse microphotographs show microglial (red) recruitment by AD Neu + AC (green) compare to control (Neu + AC; green). Scale bars, 250 μm (top) and 200 μm (bottom three rows). **b**, Microglia are ramified (resting) on day 0 in the angular chambers, become elongated (motile) on day 2, and migrate along the microchannels toward the central chamber. All experiments were repeated ≥3 times. Scale bars, 10 μm. **d**,**c**, Both the length (**c**) and level (**d**) of CD11b expression increase in the motile microglia ($F_{1,14} = 564.7$; unpaired, two-sided Student's *t* test, $n = 10$ cells at day 4 culture condition). All experiments were repeated ≥3 times. **e**, Triculture in the 3D Neu + AC + MG AD model (red) leads to a dramatic increase in microglia recruitment, as measured by the total number of microglia accumulated in the central chamber compared to the 3D Neu + AC + MG control (blue) and the 2D Neu + AC + MG AD model (purple; $R^2 = 0.9745$, $F_{2,12} = 228.9$; unpaired, two-way ANOVA, $n = 5$ devices per culture condition). All experiments were repeated ≥3 times. RI, microglial recruitment index. **f**,**g**, The 3D Neu + AC + MG AD also produced discernible amounts of (**f**) chemokines and (**g**) pro-inflammatory soluble factors ($F_{7,21} = 115.6$; two-way ANOVA, $n = 4$ devices per culture condition). All experiments were repeated ≥3 times. $^{**}P < 0.001$, $^{***}P < 0.0001$; *, not detected; $n = 5$ devices in **a**,**e**–**g** and $n = 100$ cells each in **b**–**d**. All data are presented as mean ± s.e.m.

models. For this purpose, we first measured the secreted cytokine and chemokine levels in 3D Neu + AC and 3D Neu + AC AD models without microglial cells. Conditioned cell culture media were collected from the week 9 models and levels of 36 cytokines were analyzed. Notably, protein levels of CCL2, CXCL10, and CX3CL1 were substantially increased in 3D Neu + AC AD compared to the control 3D Neu + AC model (Fig. 3f). In contrast, no changes in CCL3/4, CCL5, and CXCL1 expression were found in either culture model. Next, we assessed how inflammatory signaling was impacted by adding microglial cells to the 3D Neu + AC AD model. AD-related neuroinflammatory responses, such as chemokine release (Fig. 3f) and pro-inflammatory factor secretion (Fig. 3g and Supplementary Fig. 13), were generally increased by the addition of microglial cells. Indeed, IL-6, IL-8, and TNF-α concentrations were elevated by 2.2-, 2.7-, and 1.3-fold, respectively, compared to 3D Neu + AC AD alone. In addition, activated microglia induced the release of multiple chemokines including CCL2 (2.1-fold), CCL5 (26-fold), CXCL10 (2.6-fold), and CXCL12 (1.2-fold) in 3D Neu + AC + MG AD compared to the 3D Neu + AC AD. We also observed production of the leukocyte growth factors GM-CSF and G-CSF, which typically are not produced by neurons. MIF and PAI-1, important biomarkers of tau hyperphosphorylation in late-stage AD mouse model, were greatly increased in 3D Neu + AC + MG AD (Fig. 3g)[31]. Secretion of inflammtory cytokines such as IL-1β and IL-17 and anti-inflammatory markers such as IL-1RA, IL-10, and TGF-β was very limited or below detectable levels. These data suggest that microglia elicit broad inflammatory signaling in response to our 3D Neu + AC AD model.

Recruited microglia are toxic to AD neurons and astrocytes. Next, we assessed the extent of cellular damage mediated by microglia in our 3D Neu + AC + MG AD culture model. On day 2, after adding microglial cells to 9-week-differentiated 3D Neu + AC AD system, we observed morphological changes of microglial cells co-localized with GFP$^+$ 3D Neu + AC AD cells (Fig. 4a and Supplementary Video 6). After day 4, we observed slight decreases in neuron/astrocyte surface area, including cell body and axon, when co-localized with microglia (Fig. 4a). Axonal damages were also observed with co-localized microglial cells (Fig. 4b, Supplementary Fig. 14, and Supplementary Video 7). Time-lapse imaging also indicated that AD neurons underwent changes in cell morphology, including retraction of the neurites toward the main cell bodies (Fig. 4c and Supplementary Video 8). To quantitatively analyze the cellular damages, we next performed image analysis by converting nucleus-stained images into a dimension matrix to determine nucleus density in triculture conditions with microglia via heat map contours (Fig. 4d and Supplementary Fig. 15). At day 2, cells exhibited relatively moderate density across regions of interest (ROIs). However, at day 6, a marked decrease of cellular density was observed around nearby microglia cells (Fig. 4e). Indeed, after day 6 of triculture with microglial cells, there was a 21% reduction in Neu + AC survival counted by nucleus (Fig. 4e) and a marked reduction of about 37% in Neu + AC surface area (Fig. 4f) when tricultured with microglia compared to 9-week-old 3D Neu + AC AD only (Supplementary Fig. 15). To elucidate and quantify how microglia influence the induction of neuronal and/or astrocyte loss, we analyzed 9-week-old 3D Neu + AC + MG AD at day 2 and day 6 after microglial cell recruitment using immunostaining and immunoblotting to compare and quantify the loss of each cell type (Fig. 4g,h). TUJ1 and MAP2 (neurons) and ALDH1L1 (astrocyte) markers were used to quantify the neuron and astrocyte loss. Our data indicated broad losses of neurons (Tuj1, 35.5%; MAP2, 27.9%) and astrocytes (15.7%) across all 3D Neu + AC + MG AD models tested, whereas the number of microglia (CD68$^+$) remained the same (Fig. 5e). Our results, therefore, suggest that the addition of microglial cells promotes distinct changes in the number and morphology of neurons/astrocytes, which is consistent with the neuropathological findings previously demonstrated in the 5xfAD mouse model[32].

Recruited microglia induced neuronal loss through a IFN-γ- and TLR4-dependent mechanism. To test whether cytokines and chemokines contribute to neuron and astrocyte loss, we evaluated the contribution of IFN-γ and TLR4 on the production of neurotoxic mediators in our triculture system (Fig. 5a). TNF-α and NO concentrations were measured in the presence of either neutralizing or blocking antibodies to IFN-γ or TLR4, respectively[33]. Recruited microglia in the 3D Neu + AC + MG AD model exhibited a 2.3-fold increase in TNF-α concentrations compared to the 3D Neu + AC AD model without microglia (Fig. 5b). NO levels were also increased by 9.1-fold in the 3D Neu + AC + MG AD model, while not detectable in the 2D Neu + AC + MG AD model, possibly due to lack of IFN-γ in this system (Figs. 2g and 5c). Addition of either TLR4- or IFN-γ-neutralizing antibodies reduced TNF-α and NO concentrations, demonstrating that the neuron/astrocyte loss in 3D Neu + AC + MG AD is dependent on microglial activation. We also measured lactate dehydrogenase (LDH) release in conditioned media as a biochemical marker of cell death (Fig. 5d). Notably, incubation with the TLR4 antagonist LPS-RS substantially decreased LDH levels in the 3D Neu + AC + MG AD culture model (Fig. 5d). These data suggest that the microglia-induced neuronal loss in the 3D Neu + AC + MG AD model occurs at least partially via IFN-γ- and TLR4-dependent mechanisms, in agreement with the other models[33].

We also observed increased GFAP signals and altered astrocyte morphology in the 3D Neu + AC AD and Neu + AC + MG AD models, suggestive of astrogliosis (Fig. 5e). Both 3D Neu + AC AD and Neu + AC + MG AD models induced astrogliosis in week 9, as indicated by increased GFAP expression. Furthermore, astrocyte activation was concomitant with activation of microglia, as indicated by increases in CD68 immunoreactivity and thickening of their processes, indicative of a shift in state toward a more activated amoeboid morphology (Fig. 5e). Additionally, we observed that some of the neuronal loss was associated with the activation of apoptotic pathways, as we observed fragmented nuclei after 8 h in 3D Neu + AC + MG AD (Fig. 5f).

Knocking down TLR4 expression provided protection against neurotoxic microglial activation. Since we observed a reduction in TNF-α and NO concentrations following the addition of TLR4-blocking antibodies, we hypothesized that TLR4 activity is required for microglial activation. Thus, we investigated whether selective knockdown of TLR4-receptor expression can similarly reduce the inflammatory status of microglia in our AD models. To test this, we used lentiviral particles to knock down TLR4 in wild-type (WT) microglial cells (TLR4-knockdown) and plated these cells in the angular chamber. TLR4-knockdown microglial cells exhibited a 79% decrease in TLR4 compared to WT microglial cells (Fig. 5g). Knocking down TLR4 in microglial cells protected against neuron and astrocyte loss (2.3-fold) compared to WT microglial cells in the 3D Neu + AC + MG AD systems.

Human iPSC-derived AD Neu+AC replicate microglial recruitment, activation, and Neu+AC death in triculture. To confirm that the proposed mechanism can be replicated in other cultured human neurons/astrocytes, we newly generated human iPSC-derived neural stem cells (NSCs) expressing high levels of pathogenic Aβ species using techniques similar to those used for the ReNcell VM-based 3D AD models (Fig. 6a). Human NSCs, stably expressing APPSL and GFP (AD iPSCs) or GFP alone (control iPSCs), were plated and differentiated for 3 weeks under 3D culture conditions. In these culture conditions, we also confirmed that cells were differentiated into neurons and astrocytes, respectively, as determined by the Tuj1,

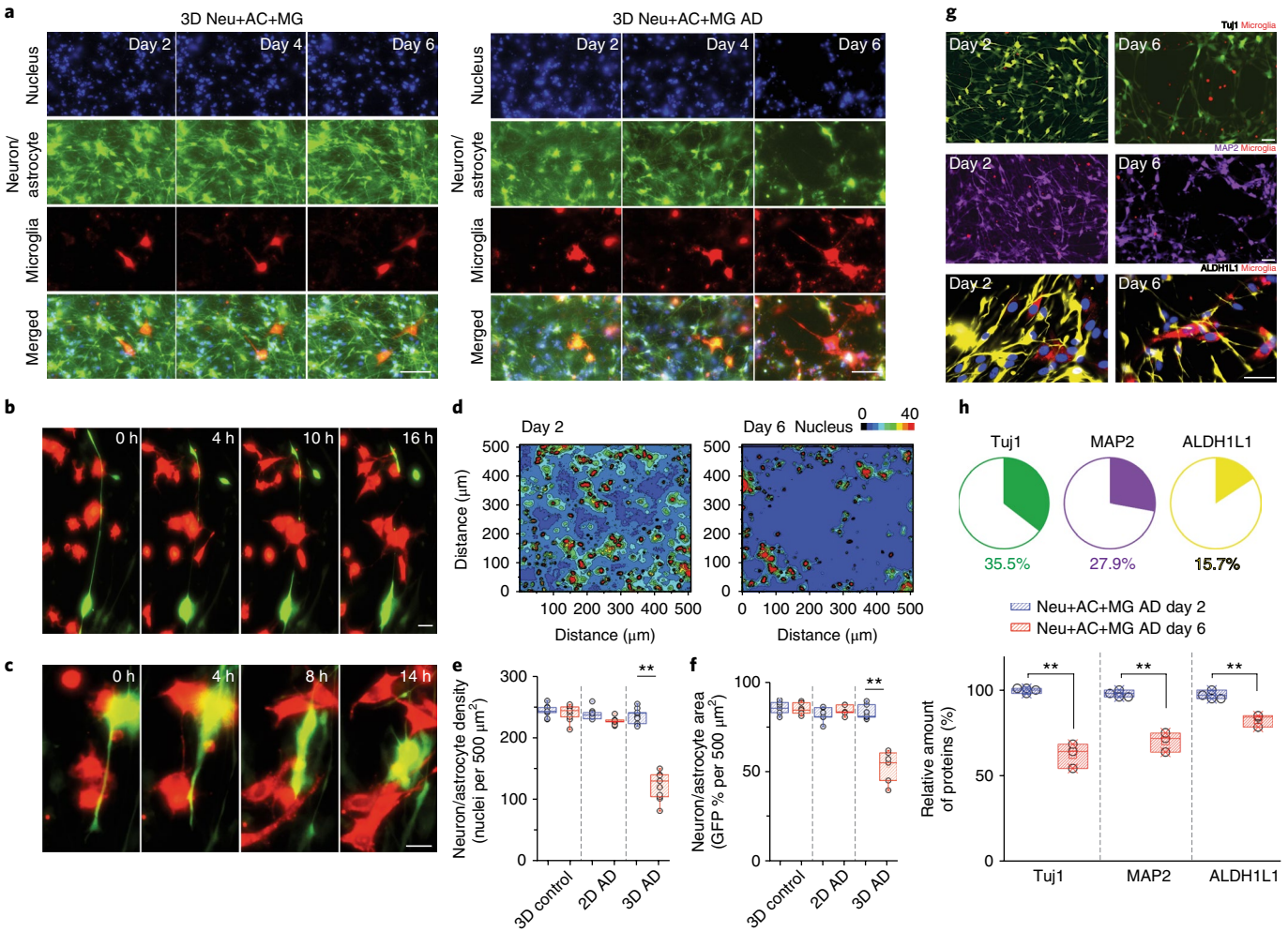

Fig. 4 | Neuronal damage is exacerbated through interactions with reactive microglial cells. a–c, Time-lapse microphotographs highlight the neurotoxic interactions among recruited microglia (red) and AD neurons/astrocytes (green) with nucleus staining (blue) in a real time: (**a**) gradual depletion of neurons/astrocytes from day 2 to day 6, (**b**) axonal cleavage, and (**c**) retraction of neuronal neurite (16 h of observation) in microglial co-localizing regions of interest (ROIs) of 3D Neu + AC + MG AD model compared to a control (3D Neu + AC + MG). Scale bars, 80 μm in **a** and 10 μm in **b**,**c**. **d**, Localized neuronal damage proximate to the recruited microglia is visualized on a contour heat map. All experiments were repeated ≥3 times. **e**,**f**, Neuronal loss is quantified by measuring (**e**) the number of nuclei and (**f**) GFP-overlaying surface areas of neurons/astrocytes in the 3D Neu + AC (3D control), the 2D Neu + AC AD (2D AD), and 3D Neu + AC AD (3D AD) in the absence (blue) and the presence of microglia (red). **g**, Cell types identified by immunostaining specific markers (Tuj1, green; MAP2, purple; ALDH1L1, yellow). Scale bars, 80 μm (Tuj1 and MAP2) and 10 μm (GFAP). **h**, Numbers of surviving neurons/astrocytes compared between day 2 and day 6 after microglial recruitment ($F_{1,6} = 95.12$; two-way ANOVA with Tukey–Kramer test). $^{**}P < 0.0001$ with $n = 20$ images each in **d**–**f** and $n = 5$ devices each in **d**–**f**,**h**. All data are presented as mean ± s.e.m.

MAP2, and GFAP immunofluorescence staining (Fig. 6b,c). To further examine the development of synapse-like structures, dendritic protrusions at week 0 and week 3 were compared (Fig. 6d,e). In particular, we imaged these protrusions making connections between synapses-like structures in the volume (Fig. 6f). As expected, the 3D Neu + AC + MG AD iPSC culture produced high levels of Aβ40 (1.75 ng/mL) and Aβ42 (0.45 ng/mL; Fig. 6g). We also analyzed the cytokine secretion profile at week 3. Incubating 3D Neu + AC AD iPSC for 3 weeks led to increased cytokine and chemokine secretion. Indeed, the release of inflammation-related CCL2, CCL5, IL6, IL8, and MIF were upregulated following the addition of microglial cells (Fig. 6h). Notably, IL-1β, IL-6, IL-10, and TNF-α were not detected in the 3D Neu + AC AD iPSC cultures without microglia (Fig. 6h). Crucially, microglial migration and recruitment was largely elevated in the 3D Neu + AC + MG AD iPSCs as compared to in 3D Neu + AC + MG control iPSCs (Fig. 6i–j). We next treated 3D Neu + AC + MG AD iPSC with IFN-γ and compared the neuron/astrocyte loss between AD and control cells. 3D Neu + AC + MG AD iPSCs showed substantially higher levels of neuron/astrocyte loss, while the IFN-γ-neutralizing antibody treatments protected against neuron/astrocyte loss (Fig. 6k,l). These data further validated our findings on glial activation and the role of cytokines in 3D triculture models with iPSC-derived human neuron/astrocyte cells.

In conclusion, we were able to recapitulate dynamic neural–glial interactions in a 3D human triculture (Neu + AC + MG) system. This model was generated by differentiating genetically modified human NPCs into neurons and astrocytes, expressing AD pathological hallmarks: Aβ aggregation, p-tau formation, and chemokine and cytokines such as CCL2, TNF-α, and IFN-γ. We achieved this by co-culturing on a microfluidic platform and by triculturing human adult microglia in separated angular chambers to observe microglia recruitments with AD neuron and astrocytes. The relevance of this triculture model lies in the demonstration of physiologically relevant neural–glial interactions: microglial morphogenesis, recruitment, the release of proinflammatory cytokines and leukocyte

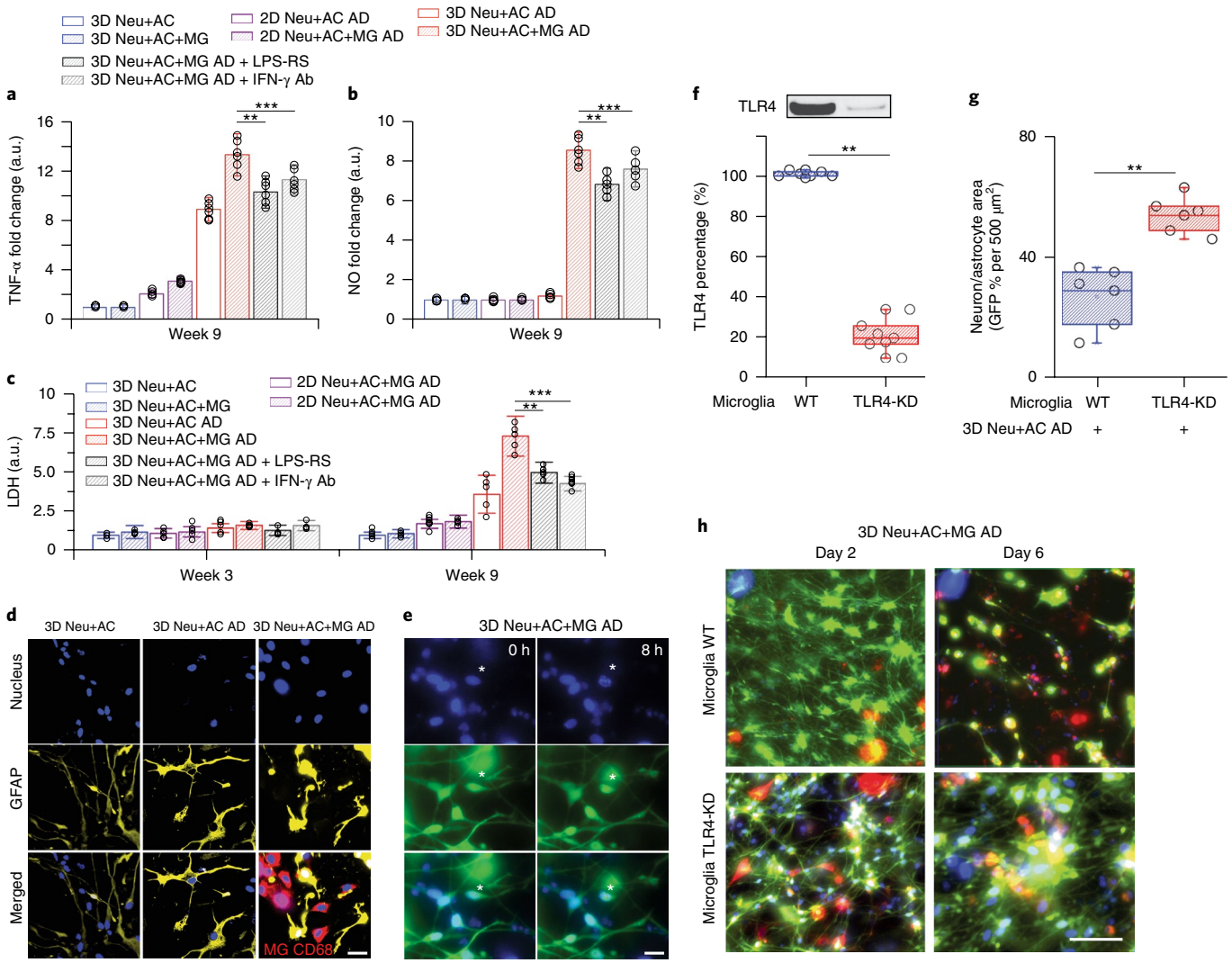

Fig. 5 | Assessment of neurotoxic neuron–glia interactions mediated by TLR4 and IFN-γ receptor. a,**b**, In triculture, 3D Neu + AC + MG AD express elevated levels of (**a**) TNF-α and (**b**) NO compared to controls (3D Neu + AC + MG and 2D and 3D Neu + AC AD) and treatment using either TLR4 antagonist or blocking IFN-γ antibody reduced the concentrations of TNF-α and NO ($R^2 = 0.9024$, $F_{4,10} = 1.061$, $F = 23.11$; two-way ANOVA). All experiments were repeated ≥3 times. **c**, In 3D Neu + AC + MG AD after 9 weeks of differentiation, neurotoxic interactions were mimicked by LDH concentrations ($R^2 = 0.7104$, $F_{1,14} = 15.65$); the damage was attenuated through inhibition using a TLR4 antagonist and a blocking IFN-γ antibody (f; $R^2 = 0.8954$, $F_{1,14} = 22.61$). **d**, Immunostaining of the astrocyte marker GFAP (yellow) and microglial CD68 (red) demonstrated activation of astrocytes and microglia in 3D Neu + AC AD and 3D Neu + AC + MG AD compared to 3D Neu + AC. Scale bar, 10 μm. **e**, Apoptotic cells with fragmented nuclei observed after 8 h, marked by * in 3D Neu + AC + MG AD. Scale bar, 10 μm. **f**, Immunoblot and quantification of proteins isolated from WT and TLR4-knockdown (TLR4-KD) microglia. Fold changes were determined by normalizing the TLR4 band intensity to Actin ($R^2 = 0.8934$, $F_{1,3} = 21.65$). **g**,**h**, Reduced Neu + AC loss was (**g**) measured with GFP-overlaying surface area ($R^2 = 0.8240$, $F_{1,3} = 19.25$) and (**h**) visualized with fluorescent microphotographs in 3D Neu + AC AD with TLR4-KD microglia. All experiments were repeated ≥3 times. Scale bar, 40 μm. Statistics reflect two-way ANOVA; IFN-γ vs. IFN-γ + Aβ, $^{\#}P < 0.0002$; Aβ vs. IFN-γ + Aβ, $^{\dagger}P < 0.0002$; IFN-γ + Aβ vs. IFN-γ + Aβ + TLR4 Ab, $^{\#*}P < 0.0002$; IFN-γ + Aβ vs. IFN-γ + Aβ + LPS-RS, $^{\dagger*}P < 0.0002$ and $^{**}P < 0.001$, $^{***}P < 0.0001$ with $n = 5$ wells in **a**,**b**, $n = 5$ devices in **c**–**e**. All data are presented as mean ± s.e.m.

chemokines regulated by AD neurons and astrocytes, and microglial neurotoxic activation contributing to neuron/astrocyte damage. These findings carry important implications for studies aimed at a deeper understanding of the gliosis and pathogenesis of AD and for screens aimed at finding new therapeutic molecules for preventing and treating AD.

Discussion

Relevant in vitro models of human AD brain must be capable of recapitulating all three pillars of AD pathology: Aβ accumulation, p-tau aggregation, and neuroinflammation. Human neurons derived from Alzheimer's disease patients have shown elevated levels of toxic Aβ species and phosphorylated tau. However, current AD neuronal models do not include neuroinflammatory changes that are mediated by microglial cells. To overcome this limitation, we developed a triculture system of neurons, astrocytes, and microglia that can achieve microglial recruitment, secretion of pro-inflammatory cytokines and chemokines, and neuron/astrocyte loss. The generation of this in vitro human AD culture model will provide more a physiologically relevant system to address key pathological features in AD.

Derived from 3D culture platforms, the microfluidic model presented a more physiologically relevant brain environment characterized by increased expression of neuronal (Tuj1, MAP2) and

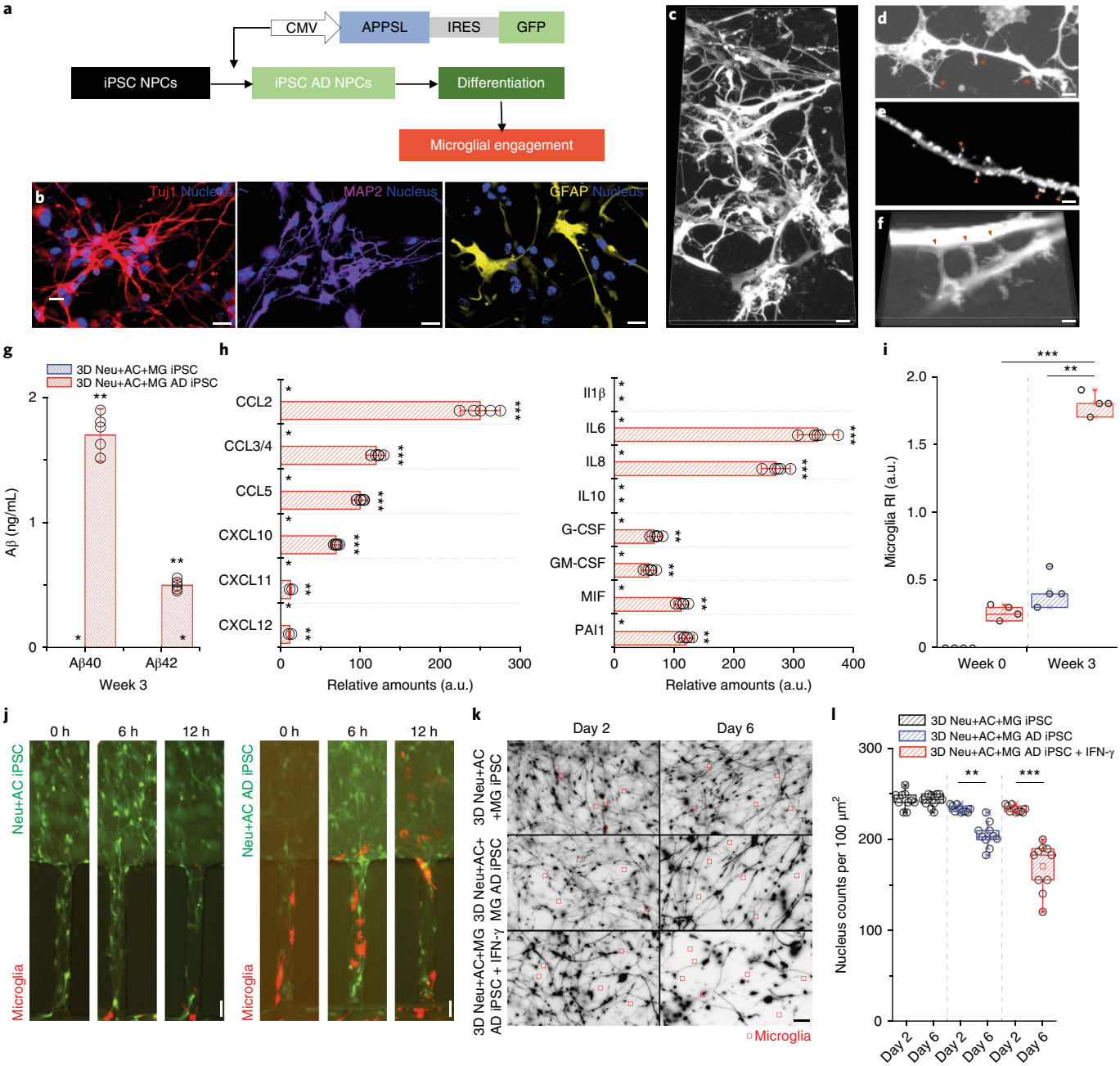

Fig. 6 | Neuron–glia interactions recapitulated with human iPSC-derived AD neurons/astrocytes. a, Schematics describing the procedure used to generate iPSC AD NPCs and illustrating the plating. **b**, Immunofluorescent microphotographs validate the differentiated neuron (blue, nucleus) with class III β-tubulin Tuj1 (red) and MAP2 (purple), astrocytes (blue, nucleus) with GFAP (yellow) following 3 weeks of differentiation. Scale bar, 20 μm. **c**–**f**, Representative microphotographs of differentiated neurons/astrocytes show (**c**) an overview, (**d**) protrusion of dendritic spines, (**e**) synaptic boutons, and (**f**) connections. Scale bar, 20 μm (**c**); 5 μm (**d**–**f**). **g**, 3D Neu + AC + MG AD iPSCs express elevated levels of Aβ40 and Aβ42 compared to controls (3D Neu + AC + MG iPSC; $F_{2,4} = 125.6$; $n = 5$ devices). All experiments were repeated ≥3 times. *, not detected. **h**, The 3D Neu + AC + MG AD iPSCs also produce discernible amounts of chemokines (left) and pro-inflammatory soluble factors (right; $F_{1,22} = 321.3$; $n = 5$ devices). **i**,**j**, Triculture in 3D Neu + AC + MG AD iPSCs (red bars in **i**; right microphotographs in **j**) leads to a dramatic increase in microglia recruitment as measured by the total number of microglia accumulated in the central chamber compared to the 3D control (blue bars in **i**, left micrographs in **j**; $R^2 = 0.7954$, $F_{2,12} = 199.7$; unpaired, two-way ANOVA; $n = 5$ devices per culture condition). All experiments were repeated ≥3 times. Scale bar, 10 μm. **k**, Representative microscopic images show the reduced density of neurons/astrocytes tricultured with microglia (red squares) after microglial engagement for 2 d and 6 d. Scale bar, 20 μm. **l**, Numbers of surviving neurons/astrocytes measured in 3D Neu + AC AD iPSCs treated with IFN-γ compared with untreated controls (3D Neu + AC + MG iPSCs and 3D Neu + AC AD iPSCs; $R^2 = 0.9731$, $F_{1,10} = 17.45$; two-way ANOVA;). $^{**}P < 0.001$, $^{***}P < 0.0001$. All data are presented as mean ± s.e.m.

astrocyte (GFAP) markers as compared to 2D systems, in agreement with previous reports[15]. Maturation of these neurons/astrocytes in 3D could result from several mechanisms: (i) materials whose properties closely mimic those of the in vivo extracellular matrix have been shown to promote differentiation of progenitor cells into the mature phenotypes[25] and/or (ii) the 3D environment provides a large surface area for growth and differentiation[26]. Notably, in contrast to previously developed AD-derived iPSCs that only showed

early-stage AD signatures, at week 9 our 3D triculture model mimics late-stage AD markers, i.e., robust increases in p-tau formation. Moreover, the 3D triculture model secretes cytokines and chemokines such as TNF-α, IFN-γ, and MCP-1. The clinical relevance of these findings is supported by a marked upregulation of TNF-α in APP AD transgenic mice and by an increased expression of IFN-γ in AD brain tissue. IFN-γ is released predominantly by Aβ-activated immune cells[33,34] and TNF-α-activated astrocytes[35–37] and binds to IFN-γ receptors, which are abundant and functionally present on microglia[38]. Taken together, these findings provide evidence that the combination of neurons, astrocytes, and microglia in 3D culture accelerates pathogenic cascades of AD, thus representing a suitable model for the study of AD mechanisms.

The role of chemokines in the recruitment of microglia in AD brain is not fully known. To identify the mechanism(s) of microglial accumulation into AD brain, we added adult microglia cells in a separate angular chamber connected to the precultured neuronal/astrocyte central chamber. Microglial recruitment was substantially higher in the 3D Neu+AC+MG AD as compared to 3D control or 2D AD microenvironments. Although the higher recruitment in the 3D Neu+AC+MG AD neuron is likely due to a combination of many factors, three major elements contributed to the increase in microglia recruitment. First, Aβ accumulation affected the increase of microglia recruitment. In our previous study, we demonstrated that soluble Aβ served as a 'recruiting signal' for microglia[39]. 3D Neu+AC+MG AD was cultured for 9 weeks; thus, greater levels of Aβ were present in either 3D gel media or conditioned media. Second, 3D Neu+AC AD secreted key recruiting chemokines, such as CCL2/MCP-1, which is upregulated in human AD brains. CCL2/MCP-1 is produced mainly by cultured microglia[29] and astrocytes[40]. Indeed, neutralizing antibodies against CCL2/MCP-1 substantially inhibited the migration of microglia. CXCL10 induced migration and a proinflammatory phenotype in cultured microglia and T cells[41]. Finally, conditioned media from 6- and 9-week 3D Neu+AC+MG AD cultures showed increased adenosine triphosphate (ATP) levels, which likely promoted microglial activation or chemotaxis[42]. Microglia also express several purinoceptors, including a Gi-coupled subtype that has been implicated in ATP- and adenosine diphosphate (ADP)-mediated migration in vitro[43]. An increase of extracellular ATP levels during AD progression has been reported in a murine model of the disease[44]. These data highlight the relevance of our 3D Neu+AC+MG AD neuron model for studying key factors driving microglia recruitment or for studying the expression of surface markers contributing to migration. Moreover, 3D Neu+AC AD-secreted Aβ and MCP-1 can both generate molecular gradients affecting microglial activation and alter their phenotype[39]. Changes in their phenotypes showed a trend for CD11b upregulation and correlated more closely with measures of the M1-like phenotype[45].

In addition to neurotoxic soluble factors, activated microglia have been shown to contribute to neuronal synapse engulfment by physical contact in AD mouse models, including C1q upregulation via the classical complement system[46]. In our 3D culture model, we observed physical interruptions between neurons and microglia, i.e., cleaved axons and retraction of neurite with co-localized microglia. While we could not determine whether microglia regulate synapses in our model, this observation demonstrated that our model will allow the study of neuronal loss associated with microglia physical interactions.

It should be noted that an immortalized microglia cell line, transformed with simian virus 40 (SV40) T antigen, was used in our studies. Extending these studies using human iPSC-derived microglia as well as primary microglia will be helpful to confirm our findings. Future studies incorporating AD-risk-associated innate immune genotypes, for example, *CD33* and *TREM2*, in 3D mixed neural–glial cultures should be another application.

In conclusion, our 3D AD culture model represents a substantial improvement over current in vitro human AD models by adding inflammatory activity. Although physiologically relevant in vivo studies will ultimately be needed to confirm the clinical utility of our model, success of this 3D triculture modeling should foster a greater understanding of the molecular mechanisms underlying gliosis and pathogenesis, as well as more effective screening for therapies aimed at slowing, stopping, or reversing neurodegeneration in AD.

Methods

Methods, including statements of data availability and any associated accession codes and references, are available at https://doi.org/10.1038/s41593-018-0175-4.

Received: 17 March 2017; Accepted: 25 May 2018;
Published online: 27 June 2018

References

1. Alzheimer's Association. 2016 Alzheimer's disease facts and figures. *Alzheimers Dement.* **12**, 459–509 (2016).
2. Tanzi, R. E. & Bertram, L. Twenty years of the Alzheimer's disease amyloid hypothesis: a genetic perspective. *Cell* **120**, 545–555 (2005).
3. Karran, E. & De Strooper, B. The amyloid cascade hypothesis: are we poised for success or failure? *J. Neurochem.* **139**, 237–252 (2016). Suppl 2.
4. Armstrong, R. A. A critical analysis of the 'amyloid cascade hypothesis'. *Folia Neuropathol.* **52**, 211–225 (2014).
5. Paquet, D. et al. Efficient introduction of specific homozygous and heterozygous mutations using CRISPR/Cas9. *Nature* **533**, 125–129 (2016).
6. Tubsuwan, A. et al. Generation of induced pluripotent stem cells (iPSCs) from an Alzheimer's disease patient carrying a L150P mutation in *PSEN-1*. *Stem Cell Res.* **16**, 110–112 (2016).
7. Moore, S. et al. APP metabolism regulates tau proteostasis in human cerebral cortex neurons. *Cell Rep.* **11**, 689–696 (2015).
8. Muratore, C. R. et al. The familial Alzheimer's disease APPV717I mutation alters APP processing and Tau expression in iPSC-derived neurons. *Hum. Mol. Genet.* **23**, 3523–3536 (2014).
9. Sproul, A. A. et al. Characterization and molecular profiling of PSEN1 familial Alzheimer's disease iPSC-derived neural progenitors. *PLoS One* **9**, e84547 (2014).
10. Kondo, T. et al. Modeling Alzheimer's disease with iPSCs reveals stress phenotypes associated with intracellular Aβ and differential drug responsiveness. *Cell Stem Cell* **12**, 487–496 (2013).
11. Yagi, T. et al. Establishment of induced pluripotent stem cells from centenarians for neurodegenerative disease research. *PLoS One* **7**, e41572 (2012).
12. Koch, P. et al. Presenilin-1 L166P mutant human pluripotent stem cell-derived neurons exhibit partial loss of γ-secretase activity in endogenous amyloid-β generation. *Am. J. Pathol.* **180**, 2404–2416 (2012).
13. Shi, Y. et al. A human stem cell model of early Alzheimer's disease pathology in Down syndrome. *Sci. Transl. Med.* **4**, 124ra29 (2012).
14. Israel, M. A. et al. Probing sporadic and familial Alzheimer's disease using induced pluripotent stem cells. *Nature* **482**, 216–220 (2012).
15. Choi, S. H. et al. A three-dimensional human neural cell culture model of Alzheimer's disease. *Nature* **515**, 274–278 (2014).
16. Kim, Y. H. et al. A 3D human neural cell culture system for modeling Alzheimer's disease. *Nat. Protoc.* **10**, 985–1006 (2015).
17. D'Avanzo, C. et al. Alzheimer's in 3D culture: challenges and perspectives. *BioEssays* **37**, 1139–1148 (2015).
18. Choi, S. H., Kim, Y. H., Quinti, L., Tanzi, R. E. & Kim, D. Y. 3D culture models of Alzheimer's disease: a road map to a "cure-in-a-dish". *Mol. Neurodegener.* **11**, 75 (2016).
19. Heneka, M. T. et al. NLRP3 is activated in Alzheimer's disease and contributes to pathology in APP/PS1 mice. *Nature* **493**, 674–678 (2013).
20. Griciuc, A. et al. Alzheimer's disease risk gene *CD33* inhibits microglial uptake of amyloid beta. *Neuron* **78**, 631–643 (2013).
21. Butovsky, O. et al. Identification of a unique TGF-β-dependent molecular and functional signature in microglia. *Nat. Neurosci.* **17**, 131–143 (2014).
22. Crehan, H., Hardy, J. & Pocock, J. Blockage of CR1 prevents activation of rodent microglia. *Neurobiol. Dis.* **54**, 139–149 (2013).
23. Guerreiro, R. et al. TREM2 variants in Alzheimer's disease. *N. Engl. J. Med.* **368**, 117–127 (2013).
24. Xu, Q., Li, Y., Cyras, C., Sanan, D. A. & Cordell, B. Isolation and characterization of apolipoproteins from murine microglia. Identification of a low density lipoprotein-like apolipoprotein J-rich but E-poor spherical particle. *J. Biol. Chem.* **275**, 31770–31777 (2000).
25. Zhang, Z.-N. et al. Layered hydrogels accelerate iPSC-derived neuronal maturation and reveal migration defects caused by MeCP2 dysfunction. *Proc. Natl. Acad. Sci. USA* **113**, 3185–3190 (2016).

26. Han, S. et al. Three-dimensional extracellular matrix-mediated neural stem cell differentiation in a microfluidic device. *Lab Chip* **12**, 2305–2308 (2012).
27. Tischbirek, C., Birkner, A., Jia, H., Sakmann, B., & Konnerth, A. Deep two-photon brain imaging with a red-shifted fluorometric Ca^{2+} indicator. *Proc. Natl. Acad. Sci. USA* **112**, 11377–11382 (2015).
28. El Khoury, J. B. et al. CD36 mediates the innate host response to β-amyloid. *J. Exp. Med.* **197**, 1657–1666 (2003).
29. El Khoury, J. et al. Ccr2 deficiency impairs microglial accumulation and accelerates progression of Alzheimer-like disease. *Nat. Med.* **13**, 432–438 (2007).
30. Brion, J. P. Neurofibrillary tangles and Alzheimer's disease. *Eur. Neurol.* **40**, 130–140 (1998).
31. Li, S.-Q. et al. Deficiency of macrophage migration inhibitory factor attenuates tau hyperphosphorylation in mouse models of Alzheimer's disease. *J. Neuroinflamm.* **12**, 177 (2015).
32. Spangenberg, E. E. et al. Eliminating microglia in Alzheimer's mice prevents neuronal loss without modulating amyloid-β pathology. *Brain* **139**, 1265–1281 (2016).
33. Papageorgiou, I. E. et al. TLR4-activated microglia require IFN-? to induce severe neuronal dysfunction and death in situ. *Proc. Natl. Acad. Sci. USA* **113**, 212–217 (2016).
34. Browne, T. C. et al. IFN-γ production by amyloid β-specific Th1 cells promotes microglial activation and increases plaque burden in a mouse model of Alzheimer's disease. *J. Immunol.* **190**, 2241–2251 (2013).
35. Garwood, C. J., Pooler, A. M., Atherton, J., Hanger, D. P. & Noble, W. Astrocytes are important mediators of Aβ-induced neurotoxicity and tau phosphorylation in primary culture. *Cell Death Dis.* **2**, e167 (2011).
36. White, J. A., Manelli, A. M., Holmberg, K. H., Van Eldik, L. J. & Ladu, M. J. Differential effects of oligomeric and fibrillar amyloid-β 1-42 on astrocyte-mediated inflammation. *Neurobiol. Dis.* **18**, 459–465 (2005).
37. Xiao, B. G. & Link, H. IFN-gamma production of adult rat astrocytes triggered by TNF-alpha. *Neuroreport* **9**, 1487–1490 (1998).
38. Hashioka, S., Klegeris, A., Schwab, C., Yu, S. & McGeer, P. L. Differential expression of interferon-γ receptor on human glial cells in vivo and in vitro. *J. Neuroimmunol.* **225**, 91–99 (2010).
39. Cho, H. et al. Microfluidic chemotaxis platform for differentiating the roles of soluble and bound amyloid-β on microglial accumulation. *Sci. Rep.* **3**, 1823 (2013).
40. Smits, H. A. et al. Amyloid-β-induced chemokine production in primary human macrophages and astrocytes. *J. Neuroimmunol.* **127**, 160–168 (2002).
41. Baruch, K. et al. Breaking immune tolerance by targeting Foxp3(+) regulatory T cells mitigates Alzheimer's disease pathology. *Nat. Commun.* **6**, 7967 (2015).
42. Haynes, S. E. et al. The P2Y12 receptor regulates microglial activation by extracellular nucleotides. *Nat. Neurosci.* **9**, 1512–1519 (2006).
43. Dou, Y. et al. Microglial migration mediated by ATP-induced ATP release from lysosomes. *Cell Res.* **22**, 1022–1033 (2012).
44. Perez de Lara, M. J. & Pintor, J. Presence and release of ATP from the retina in an Alzheimer's disease model. *J. Alzheimers Dis.* **43**, 177–181 (2015).
45. Johansson, J. U. et al. Suppression of inflammation with conditional deletion of the prostaglandin E2 EP2 receptor in macrophages and brain microglia. *J. Neurosci.* **33**, 16016–16032 (2013).
46. Hong, S. et al. Complement and microglia mediate early synapse loss in Alzheimer mouse models. *Science* **352**, 712–716 (2016).

Acknowledgements

We thank L. Quinti (MGH) for sharing preliminary results regarding 3D neuron/microglia co-culture systems, M. Busche (MGH) for helpful guidance regarding the calcium imaging, S.H. Choi (MGH) for helpful discussion regarding the data interpretation, and Y.J. Kang (UNCC) for critically reviewing our manuscript. This work was supported by the NIH/NIA (P01 AG015379 and RF1 AG048080 to D.Y.K. and R.E.T.; R01 AG014713 to D.Y.K.), the Pioneering Funding Award funded by Cure Alzheimer's Fund (CAF; to H.C., D.Y.K., R.E.T.), BrightFocus Foundation (D.Y.K.), the Duke Energy Special Initiatives funded by Charlotte Research Institute (CRI; to H.C.), and the Basic Science Research Program through the National Research Foundation of Korea (NRF) funded by the Ministry of Education (2015R1A6A3A03019848, to J.P.).

Author contributions

J.P. and H.C. designed, fabricated, and tested devices; designed experiments; performed immunostaining and statistical quantification; generated figures; and wrote and edited the manuscript. I.W. performed immunostaining and statistical quantification. C.D. generated human AD NPCs derived from iPSCs and measured APP and Aβ levels. D.D. and I.M. helped with confocal imaging and immunostaining, and wrote and edited the manuscript. D.Y.K., R.E.T., and H.C. conceived the ideas and directed the work, including all experiments and data analysis, and wrote and edited the manuscript. All authors read and edited the manuscript extensively.

Competing interests

The authors declare no competing interests.

Additional information

Supplementary information is available for this paper at https://doi.org/10.1038/s41593-018-0175-4.

Reprints and permissions information is available at www.nature.com/reprints.

Correspondence and requests for materials should be addressed to D.Y.K. or R.E.T. or H.C.

Publisher's note: Springer Nature remains neutral with regard to jurisdictional claims in published maps and institutional affiliations.

Methods

Media and reagents of neural progenitor cells (NPCs). ReN cell VM human neural progenitor cells (NPCs) were purchased from EMD Millipore (Billerica, MA, USA). The cells were plated onto BD Matrigel (BD Biosciences, San Jose, CA, USA)-coated T25 cell-culture flasks (BD Biosciences, San Jose, CA, USA) and maintained in DMEM/F12 (Life Technologies, Grand Island, NY, USA) media supplemented with 2 mg heparin (StemCell Technologies, Vancouver, Canada), 2% (v/v) B27 neural supplement (Life Technologies, Grand Island, NY, USA), 20 mg EGF (Sigma-Aldrich, St Louis, MO, USA), 20 mg bFGF (Stemgent, Cambridge, MA, USA), and 1% (v/v) penicillin/streptomycin/amphotericin-B solution (Lonza, Hopkinton, MA, USA) in a CO_2 cell culture incubator. Cell-culture media were changed every 3 d until cells were confluent. For 2D neuron/astrocyte differentiation, the cells were plated onto Matrigel-coated microfluidic devices with DMEM/F12 differentiation media supplemented with 2 mg heparin, 2% (v/v) B27 neural supplement, and 1% (v/v) penicillin/streptomycin/amphotericin-B solution without growth factors. One-half volume of the differentiation media was changed every 3–4 d for 3–9 weeks. LPS-RS was purchased from InvivoGen (San Diego, CA). LPS-RS was resuspended in dimethylsulphoxide (DMSO; 0.1 mg in 10 mL) followed by 1:10 dilution in differentiation culture medium. This stock solution of 22.2 mM was then diluted for cell treatment experiments.

Viral infection of NPCs. To transduce the NPCs with the lentiviral constructs, 50–100 µL viral solution (1×10^6 TU ml^{-1}, MOI = 4) were added to 85% confluent proliferating ReN cells in 6-well dishes, incubated for 24 h, and washed three times to stop the infection. The expression of the infected genes was confirmed by GFP expression by fluorescence microscopy and western blot analysis.

3D cell cultures and differentiation of NPCs. For 3D cultures, BD Matrigel (BD Biosciences) was mixed with the cells (10×10^6 cells per mL). The final cell concentration for the mixture was approximately 5×10^6 cells per mL (1:1 3D thick-culture for confocal and western blot) and 2×10^6 cells per mL (1:5 3D thin-culture for immunostaining and recruitment). We then transferred 10 µL of cell mixtures into the microfluidic device using prechilled pipettes. The microfluidic devices were incubated for 1 h at 37 °C, during which 3D gels (100–600 µm) formed and media were changed. The 3D-plated cells were differentiated for 3–9 weeks depending on the experiments; media was changed every 3–4 d. For drug treatments, differentiation media containing either 1 mM LPS-RS diluted in DMSO or the concentration of DMSO were added to 3- to 9-week differentiated 3D AD neuron–microglia cells and the 3D cultures maintained for an additional 1 week.

Expansion, viral infection, and differentiation of hiPSC-NPCs. Human iPSC derived neural progenitor cells (hiPSC-NPCs) were purchased from EMD Millipore (SCR131). The cells were plated onto BD Matrigel-coated 6-well plates (BD Biosciences, San Jose, CA, USA) and expanded in expansion medium (EMD Millipore, SCM004) supplemented with FGF-2 (20 ng/mL) and L-glutamine (2 mM) in a CO_2 cell culture incubator. To transduce the hiPSCs with the lentiviral constructs, 50–100 µL viral solution (1×10^6 TU mL^{-1}, MOI = 4) were added to 85% confluent proliferating hiPSCs in 6-well dishes, incubated for 48 h, and washed three times to stop the infection. The expression of the infected genes was confirmed by GFP expression by fluorescence microscopy and followed by FACS. To differentiate, hiPSC-NPCs were prepared approximately 10×10^6 cells per mL of Matrigel. We transferred 10 µL of cell mixtures into the microfluidic device using prechilled pipettes. The microfluidic devices were incubated for 1 h at 37 °C, during which 3D gels (100–600 µm) formed and media were changed in differentiation media (EMD Millipore, SCM017). The 3D-plated cells were differentiated for 3 weeks; media was changed every 3–4 d.

FACS enrichment of the transduced NPCs and iPSC-NPCs. The infected ReN cells were washed with DPBS and then incubated with Accutase (Millipore) for 5 min. The cell pellets were resuspended in PBS supplemented with 2% serum replacement solution (Life Technologies) and 2% B27, and then passed through a cell strainer filter (70 mm nylon, BD Biosciences). The cell concentrations were adjusted to 2×10^6 cells per mL and then enriched using a FACSAria cell sorter (Flow Cytometry Core Facility, Charlestown Navy Yard, MGH). GFP channels were used to detect the expression of the transduced genes in the individual cells. The sorted/enriched cells were maintained in normal proliferation media.

Microfluidic device fabrication. Negative photoresists SU-8 50 and SU-8 100 (MicroChem, Newton, MA, USA) were sequentially patterned using standard lithography on a 4-inch (10.16-cm) silicon wafer to create a mold for cell migration channels of 50 µm height and chemokine compartments of 100 µm height. The base and a curing agent were mixed at a 10:1 weight ratio (SYLGARD 184 A/B, Dow corning, Midland, MI, USA), poured onto the SU-8 mold, and cured for 1 h at 25 °C under vacuum and, subsequently, cured for more than 3 h in an oven at 80 °C. The cured poly dimethyl-siloxane (PDMS) replica was peeled off the mold and holes were punched for fluid reservoirs. Arrayed holes were also laser-cut (Zing 24, Epilog Laser, Golden, CO, USA) into a thin PDMS membrane of 250 µm thickness (HT 6240, Bisco Silicones, Elk Grove, IL, USA) and an acrylic plate of 6 mm thickness. The machined membrane and plate were glued together using uncured PDMS and incubated at 80 °C overnight. This assembly was irreversibly bonded, first to the PDMS replica using oxygen plasma at 50 mW, 5 cm, for 30 s (PX-250, March Plasma Systems, Petersburg, FL, USA), and then to a glass-bottomed Uni-Well plate (MGB001-1-2-LG, Matrical Bioscience, Spokane, WA, USA). Immediately after the bonding, 10 µL of poly-L-lysine solution (PLL, M.W. 70,000–150,000, 1.0 mg/mL, Sigma-Aldrich Co. LLC, St. Louis, MO, USA) were injected into each platform, and it was incubated for 2 h at 25 °C to promote cellular adhesion. The PLL-treated surface was rinsed with autoclaved and 0.2-µm filtered water (AM9920, Life Technologies, Grand Island, NY, USA).

Calcium imaging. To assess neural activity, cellular calcium dynamics was monitored using Rhod-2 (Life Technologies), a Ca^{2+} indicator. Neuron-cultured samples were incubated for 30 min at 37 °C in artificial buffered cerebrospinal fluid (i.e., 25 mM $NaHCO_3$, 25 mM D-glucose, 125 mM NaCl, 2.5 mM KCl, 1.25 mM NaH_2PO_4, 1 mM $MgCl_2$, and 2 mM $CaCl_2$) supplemented with 2 M of OGB-1 diluted in pluronic F-127 20% solution/DMSO (Sigma). After incubation, the samples were washed twice with fresh artificial buffered cerebrospinal fluid and incubated for 30 min at 37 °C. Fluorescence intensity dynamics was measured using time-lapse imaging (Texas red filter cube; 20× objective; Nikon microscope) at 30-ms frame-rates. Raw intensity values were extracted using the Nikon software suite, and relative changes in fluorescence intensity to baseline ($(F - F_0)/F_0$) were regarded as neuronal calcium signals.

Microglia preparation. The immortalized human microglia SV40 cell line, derived from primary human microglia, was purchased from Applied Biological Materials, Inc. (ABM, Inc.) and cultured in Prigrow III medium supplemented with 10% (vol/vol) FBS and 1% penicillin/streptomycin in type I collagen-coated T25-flasks (ABM, Inc.). Before the experiment, cells were washed using medium without serum and the cell membrane was labeled with red fluorescent dye (PKH26PCL, Sigma-Aldrich). Briefly, after centrifugation (400 *g* for 5 min), the cells were resuspended in 1 mL of Diluent C (G8278, Sigma-Aldrich) and immediately mixed with 4 µL of dye solution (PKH26PCL, Sigma-Aldrich). The cell/dye mixture was incubated at room temperature for 4 min and periodically mixed by pipetting to achieve a bright, uniform, and reproducible labeling. After incubation, staining was stopped by adding an equal volume (1 mL) of 1% BSA in PBS and incubating for 1 min to remove excess dye. Unbound dye was washed by centrifugation and suspending cells in culture medium (10^6 cells/mL). We injected 10 µL of the cell suspension into each platform and 100 µL of a culturing medium was added into side and central extra wells. The loaded 3D microdevices were then incubated at 37 °C supplied with 5% CO_2.

Time-lapse imaging. After microglia loading, cells were recorded using time-lapse imaging using a fully automated Nikon TiE microscope with a heated incubator to 37 °C and 5% CO_2 (10× magnification; Micro Device Instruments, Avon, MA, USA). To achieve accurate cell tracking, the maximum time resolution of acquisition was 1 frame per s.

ELISA. Aβ40 and Aβ42 levels were mainly measured using a Human/Rat Aβ ELISA Kit from Wako (Osaka, Japan). The conditioned media from undifferentiated or differentiated ReN cells were collected and diluted to 1:10 or 1:100 with a dilution buffer provided by the manufacturer. A Synergy 2 ELISA plate reader (BioTek, Winooski, VT, USA) was used to quantify Aβ40 and Aβ 42 ELISA signals. IFN-γ (DIF50) secretion was quantified in supernatants by Human Quantikine ELISA Kits (R&D Systems, Oxon, UK) according to the manufacturer's instructions.

Human cytokine array. Human Cytokine Array (ARY005) kits were used to simultaneously detect relative expression levels of 36 human cytokines (R&D Systems, Oxon, UK). Conditioned media (0.5 mL from each sample) were mixed with a cocktail of biotinylated detection antibodies. The mixture was then incubated with the Human Cytokine Array Panel A membrane. A wash step was needed to remove unbound material, and then streptavidin-HRP and chemiluminescent detection reagents were added. Light was produced at each spot in proportion to the amount of analyte bound. The positive signals on developed films were identified by placing the transparency overlay on the ChemiDoc imaging system (Bio-Rad) and aligning it with the reference spots in three corners of each array. Pixel density was analyzed with ImageJ (Wayne Rasband, NIH).

Aβ preparation. Soluble Aβ monomer was prepared by dissolving a synthesized clear human Aβ, 1-42 (4349-v, Peptide Institute, Inc., Japan) and a FITC-labeled human Aβ,1-42 (A-1119, rPeptide, Bogart, GA, USA) in DMSO at 1 mg/mL for a monomer form. Although Aβ pretreatment has generally been conducted in HFIP, because of recent reports of HFIP toxicity, Aβ was directly dissolved in DMSO according to the manufacturer's recommendations (Peptide Institute, Inc., Japan). Indeed, the slow evaporation of HFIP may trigger the formation of Aβ oligomers, which could hasten fibril formation in combination with local environmental humidity. The dissolved Aβ monomer solution was further diluted in PBS at 0.1 mg/mL and stored for up to a week at 4 °C or incubated in a shaker at 37 °C to prepare oligomeric forms.

Immunostaining. For immunofluorescent stains, we rinsed the cells and 3D cultures twice with PBS (phosphate-buffered saline). Cells were then fixed through a RT, 15–30 min incubation in fresh 4% paraformaldehyde aqueous solution (157-4, ElectronMicroscopy Sciences) followed by rinsing twice with PBS. Cells were permeabilized through incubation in 0.1% Triton X-100 in PBST (phosphate-buffered saline with 0.1% Tween 20) for 15 min at RT. Cell-specific binding was blocked through overnight incubation in 3% human serum albumin in PBST at 4 °C. After 24-h incubation with the primary antibody solutions at 4 °C, the cells were washed five times. The following antibodies (and dilutions) were used: anti-p-tau (1:40, AT8, Thermo Scientific, MN1020), anti-PHF (1:1,000, A gift from P. Davies, Albert Einstein College of Medicine), anti-GFAP (1:500, Neuromap, N206A/8), anti-MAP2 (1:200, Cell Signaling Technology, 4542), anti-CD68 (1:100, Cell Signaling, 76437), anti-Cd11b (1:100, Life Technologies, NB110-89474), anti-S100 (1:400, Abcam, ab868), anti-S100A6 (1:200, Cell Signaling, D3H3W), anti-S100B (1:500, Abcam, Ab218515), and anti-ALDH1L1 (1:200, EMD Millipore, MABN495).

Western blot analysis. Protein lysates (15–75 µg) were resolved on 12% Bis-Tris or 4–12% gradient Bis/Tris gels (Life Technologies) and the proteins were transferred to nitrocellulose membranes (Bio-Rad). For Aβ western blot analysis, the membranes were cross-linked with 0.5% glutaraldehyde solution before blocking. Western blot results were visualized using enhanced chemiluminescence (ECL). Signals were captured using ChemiDoc imaging system (Bio-Rad) and quantified using ImageJ software (NIH). The following primary antibodies were used (dilutions): anti-Aβ (1:100, 6e10; Signet), anti-Tuj1 (1:200, Abcam, ab24629), anti-MAP2 (1:200, Cell Signaling, 4542), anti-GFAP (1:100, Neuromap, N206A/8), anti-p-tau AT8 (1:30, Thermo Scientific, MN1020), anti-p-tau PHF-1 (1:200, Abcam, ab66275), anti-CD68 (1:200, BD Bioscience, 556059), anti-CD11b (1:200, EMD Millipore, MM_NF-MABF515), anti-ALDH1L1 (1:200, EMD Millipore), and Cy5 anti-mouse secondary antibody (1:400, Jackson Immunoresearch, 715-175-150).

Statistical analysis. All statistical analyses were performed using Graphpad prism software. We used either two-tailed Student's *t* tests (when comparing two groups/conditions) or one-way ANOVA followed by post hoc tests (when comparing three or more groups/conditions). Data are expressed as means ± s.e.m, and $P \leq 0.05$ was considered significant. Symbols (**, ***, #, †, #*, and †*) denote significant differences between two-group or three-group analyses. Statistical analyses are detailed in figure legends. No statistical methods were used to predetermine sample sizes, and experiments were repeated to adequately reduce confidence intervals and avoid errors in statistical testing. Data collection and analysis were not performed blind to the conditions of the experiments. Randomization was not performed, and exclusions were not made.

Reporting Summary. Further information on experimental design is available in the Nature Research Reporting Summary linked to this article.

Data and code availability. The data and software code that support the findings of this study are available from the corresponding author upon reasonable request.

Corresponding author(s): Doo Yeon Kim
Rudolph E. Tanzi
Hansang Cho

Reporting Summary

Nature Research wishes to improve the reproducibility of the work that we publish. This form provides structure for consistency and transparency in reporting. For further information on Nature Research policies, see Authors & Referees and the Editorial Policy Checklist.

Statistical parameters

When statistical analyses are reported, confirm that the following items are present in the relevant location (e.g. figure legend, table legend, main text, or Methods section).

n/a	Confirmed	
☐	☒	The exact sample size (*n*) for each experimental group/condition, given as a discrete number and unit of measurement
☐	☒	An indication of whether measurements were taken from distinct samples or whether the same sample was measured repeatedly
☐	☒	The statistical test(s) used AND whether they are one- or two-sided *Only common tests should be described solely by name; describe more complex techniques in the Methods section.*
☐	☒	A description of all covariates tested
☐	☒	A description of any assumptions or corrections, such as tests of normality and adjustment for multiple comparisons
☐	☒	A full description of the statistics including central tendency (e.g. means) or other basic estimates (e.g. regression coefficient) AND variation (e.g. standard deviation) or associated estimates of uncertainty (e.g. confidence intervals)
☐	☒	For null hypothesis testing, the test statistic (e.g. *F*, *t*, *r*) with confidence intervals, effect sizes, degrees of freedom and *P* value noted *Give P values as exact values whenever suitable.*
☒	☐	For Bayesian analysis, information on the choice of priors and Markov chain Monte Carlo settings
☒	☐	For hierarchical and complex designs, identification of the appropriate level for tests and full reporting of outcomes
☐	☒	Estimates of effect sizes (e.g. Cohen's *d*, Pearson's *r*), indicating how they were calculated
☐	☒	Clearly defined error bars *State explicitly what error bars represent (e.g. SD, SE, CI)*

Our web collection on statistics for biologists may be useful.

Software and code

Policy information about availability of computer code

Data collection	ImageJ use for the quantification of the neuron/astrocyte area in Figs. 4-6 and CellProfiler used for the counting of the microglial cells in Fig.3
Data analysis	Statistical Data was analyzed with Graphpad 6. Surface area was analyzed based on "Area Measurements of a Complex Object" which is sharing resource and can be found on website. (https://imagej.nih.gov/ij/docs/pdfs/examples.pdf) Cell counts by using CellProfiler was followed by the protocol on the website (http://cellprofiler.org/tutorials/). Specific settings of cell counts are in below: Nuclei, Typical diameter of objects: 8,20, Threshold correction factor: 1.2, Lower and upper bounds on threshold 0.04, 1.0

For manuscripts utilizing custom algorithms or software that are central to the research but not yet described in published literature, software must be made available to editors/reviewers upon request. We strongly encourage code deposition in a community repository (e.g. GitHub). See the Nature Research guidelines for submitting code & software for further information.

Data

Policy information about availability of data

All manuscripts must include a data availability statement. This statement should provide the following information, where applicable:

- Accession codes, unique identifiers, or web links for publicly available datasets
- A list of figures that have associated raw data
- A description of any restrictions on data availability

This study did not contain datasets

Field-specific reporting

Please select the best fit for your research. If you are not sure, read the appropriate sections before making your selection.

☒ Life sciences ☐ Behavioural & social sciences ☐ Ecological, evolutionary & environmental sciences

For a reference copy of the document with all sections, see nature.com/authors/policies/ReportingSummary-flat.pdf

Life sciences study design

All studies must disclose on these points even when the disclosure is negative.

Sample size	no sample sizes were predetermined with statistical methods. but our sample sizes are similar to those generally employed in the field. At least 3 devices were used in each group. Our sample sizes were sufficient to detect differences among samples
Data exclusions	Exclusion criteria for experimental data points were death of cells cause of contamination during the experimental period. No outliers were excluded in this manuscript.
Replication	For each experimental condition, at least 3 sections were analyzed per conditions and at least 3 devices were used per conditions. All attempts at replication were successful expect for the failures due to sickness or death of animals during the experimental period.
Randomization	Blocking antibodies were randomly administered to AD neuron/astrocyte/microglia tri-culture models at different weeks
Blinding	Data collections were performed together in shared microscope and the blind analysis to the conditions were performed for the each experiments.

Reporting for specific materials, systems and methods

Materials & experimental systems

n/a	Involved in the study
☐	☒ Unique biological materials
☐	☒ Antibodies
☐	☒ Eukaryotic cell lines
☒	☐ Palaeontology
☒	☐ Animals and other organisms
☒	☐ Human research participants

Methods

n/a	Involved in the study
☒	☐ ChIP-seq
☐	☒ Flow cytometry
☒	☐ MRI-based neuroimaging

Unique biological materials

Policy information about availability of materials

Obtaining unique materials	We obtained the lentiviral polycistronic vectors (CSCW-IRES-GFP) from the Massachusetts General Hospital (MGH) viral core, and these are available through the MGH viral core (https://vectorcore.mgh.harvard.edu)

Antibodies

Antibodies used	anti- Aβ (1:100, 6e10; Signet); anti-Tuj1 (1:200, Abcam, ab24629); anti-MAP2 (1:200, Cell Signaling, 4542); anti-p-tau antibody (1:40, AT8, Thermo Scientific, MN1020); anti-PHF (1:1000, A gift from P. Davies, Albert Einstein College of Medicine); anti-GFAP

	antibody (1:500, Neuromap, N206A/8), anti-MAP2 antibody (1:200, Cell Signaling Technology, 4542); anti-CD68 (1:100, Cell Signaling, 76437); anti-cd11b (1:100, Life Technologies, NB110-89474); anti-S100 (1:400, Abcam, ab868); anti-S100A6 (1:200, Cell Signaling, D3H3W); anti-S100B (1:500, Abcam, Ab218515); anti-ALDH1L1 (1:200, EMD Millipore, MABN495).
Validation	All antibodies used in this study were commercially available (excepte anti-PHF-1) and validated by companies and other studies including previous publications (Nature Protocols, Page 985, Vol 10, No 7, 2015; Nature, page 274, Vol 515, No 13, 2014)

Eukaryotic cell lines

Policy information about cell lines

Cell line source(s)	SCC008 | ReNcell VM Human Neural Progenitor Cell LIne (http://www.emdmillipore.com/US/en/product/ReNcell-VM-Human-Neural-Progenitor-Cell-LIne,MM_NF-SCC008) SCR131 | Human iPSC Derived Neural Progenitor Kit (http://www.emdmillipore.com/US/en/product/Human-iPSC-Derived-Neural-Progenitor-Kit,MM_NF-SCR131) Immortalized Human Microglia - SV40 (https://www.abmgood.com/Immortalized-Microglia-SV40-T0251.html)
Authentication	Cell line authentication was not tested
Mycoplasma contamination	Cells tested negative for mycoplasma. http://www.emdmillipore.com/US/en/product/ReNcell-VM-Human-Neural-Progenitor-Cell-LIne,MM_NF-SCC008#anchor_TI
Commonly misidentified lines (See ICLAC register)	Cells are not included in ICLAC

Flow Cytometry

Plots

Confirm that:

☒ The axis labels state the marker and fluorochrome used (e.g. CD4-FITC).

☒ The axis scales are clearly visible. Include numbers along axes only for bottom left plot of group (a 'group' is an analysis of identical markers).

☒ All plots are contour plots with outliers or pseudocolor plots.

☒ A numerical value for number of cells or percentage (with statistics) is provided.

Methodology

Sample preparation	The infected ReN cells were washed with DPBS and then incubated with Accutase (Millipore) for 5 min. The cell pellets were resuspended in PBS supplemented with 2% serum replacement solution (Life Technologies) and 2% B27, and then passed through a cell strainer filter (70 mm Nylon, BD Biosciences).
Instrument	The cell concentrations were adjusted to 2 x 106 cells per ml and then enriched by using FACSAria cell sorter (Flow Cytometry Core Facility, Charlestown Navy Yard, MGH))
Software	BD FACSDiva software
Cell population abundance	Cells are enriched and sorted either by Top 2% or 10% of transduced cells based on GFP signals. Number of events and percentile are provided in Supplementary Fig.1
Gating strategy	GFP channels were used to detect the expression of the transduced genes in the individual cells. The sorted/enriched cells were maintained in normal proliferation media

☒ Tick this box to confirm that a figure exemplifying the gating strategy is provided in the Supplementary Information.